Title	A conceptual design of spacers with hairy structures for membrane processes
Author(s)	Li, W; Chen, KK; Wang, Y; Krantz, WB; Fane, AG; Tang, C
Citation	Journal of Membrane Science, 2016, v. 510, p. 314-325
Issued Date	2016
URL	http://hdl.handle.net/10722/247297
Rights	This work is licensed under a Creative Commons Attribution-NonCommercial-NoDerivatives 4.0 International License.

Author's Accepted Manuscript

A conceptual design of spacers with hairy structures for membrane processes

Weiyi Li, Kai K. Chen, Yi-Ning Wang, William B. Krantz, Anthony G. Fane, Chuyang Y. Tang

Cite this article as: Weiyi Li, Kai K. Chen, Yi-Ning Wang, William B. Krantz, Anthony G. Fane and Chuyang Y. Tang, A conceptual design of spacers with hairy structures for membrane processes, *Journal of Membrane Science* http://dx.doi.org/10.1016/j.memsci.2016.03.021

This is a PDF file of an unedited manuscript that has been accepted for publication. As a service to our customers we are providing this early version of the manuscript. The manuscript will undergo copyediting, typesetting, and review of the resulting galley proof before it is published in its final citable form. Please note that during the production process errors may be discovered which could affect the content, and all legal disclaimers that apply to the journal pertain.

A Conceptual Design of Spacers with Hairy Structures for Membrane Processes

Weiyi Li[a], Kai K. Chen[b], Yi-Ning Wang[a], William B. Krantz[a,c], Anthony G. Fane[a,b], Chuyang Y. Tang[d*]

[a]Singapore Membrane Technology Centre, Nanyang Technological University, Singapore

[b]School of Civil and Environmental Engineering, Nanyang Technological University, Singapore

[c]Department of Chemical and Biological Engineering, University of Colorado, U.S.A.

[d]Department of Civil Engineering, the University of Hong Kong, Hong Kong SAR, China

[*]Correspondence to: Department of Civil Engineering The University of Hong Kong Pokfulam Road, Hong Kong SAR, China. Tel: +852 2859 1976 fax: +852 2559 5337. tangc@hku.hk

Abstract

The development of membrane technology requires spacers that can significantly enhance the mass-transfer rate while avoiding a severe pressure drop across the membrane module. A potential solution to this challenge is to introduce some flexible and dynamic structures into the spacer mesh. The current work was motivated to explore a conceptual design of spacers with hairy structures. The hairy structures were simulated using highly flexible nylon fibers that were fixed on a well-designed framework. The effects of fiber asymmetry and spacing on the vibrations were discussed in terms of the observations via a high speed camera. A variety of spacer prototypes were employed in a forward osmosis process to examine the performance of the hairy structures. The experimental results indicate that fiber vibrations could have a great impact on the mass transfer in the vicinity of the membrane surface and enhance the filtration flux (up to

~20%).   This fundamental study not only provides insight into the mechanisms underlying the complex fiber-flow interactions but also charts the direction for future hairy spacer design.

Keywords: Membrane processes; Spacer design; Hairy structures; Flux enhancement; Vibration spectral analysis

1. Introduction

The filtration performance of a spiral wound module (SWM) can be significantly affected by the spacers. They not only define the space between the membrane leaves, but also play a role as a turbulence promoter (some studies refer to them as an eddy promoter since the flow may not be fully developed [1, 2]). Schwinge et al. indicate that the spacer in a fluid channel can intensify the mass transfer, thereby mitigating the negative effects caused by the concentration polarization (CP) and membrane fouling [2]. It is of primary importance to optimize conventional spacers and design novel structures for better filtration performance.   Indeed, if potential improvements in membrane permeability are to be translated into higher fluxes, it will be necessary to develop spacers with better mass-transfer performance.

Early studies of spacer-filled modules concentrated on investigating the effects of the basic geometrical characteristics (e.g., mesh size, filament thickness, spacer orientation, etc.) of conventional spacers on the pressure drop and mass transfer [3-5]. These studies

2

were further refined by advanced approaches based on computational fluid dynamics (CFD) [1, 6-14] owing to the development of computational technologies. With the aid of CFD-based simulations, deeper insight was obtained to reveal the complex hydrodynamic environment in spacer-filled channels and to optimize the basic geometrical characteristics for better performance. Some novel experimental approaches were also developed to visualize the secondary flows caused by the spacers. For example, Willems et al. [15] employed particle-imaging velocimetry (PIV) to investigate the planar velocity distribution in spacer-filled channels; Gao et al. [16] developed a characterization technique based on optical coherence tomography (OCT) that is able to obtain the depth profiles of the fluid field in a unit spacer cell. As more knowledge about conventional spacers was obtained, researchers began to design novel spacers with modified structures for further enhancing filtration performance.

The modifications were initially made by changing the geometry of the filaments. Most of these ideas were borrowed from the spacer designs for heat exchangers, such as twisted tapes [17, 18]. Several novel designs specific for the spacers used in a membrane module were also reported in the past decade. For example, Schwinge et al. [19] added an additional layer of filaments into the conventional spacer mesh that consists of filaments crossing each other in two directions. The idea of this design is to reduce the void space in the fluid channel without increasing the membrane area covered by the spacer. Spacers with multilayer structures were studied by researchers from the University of Twente [20, 21]. In contrast to the designs for generating more vortices in the fluid channel, these designs were aimed at optimizing the distribution of the vortices. This is realized by sandwiching a spacer with normal or modified filaments between two

3

thinner spacers that contact the membrane surface in a more intimate manner; the middle layer diverts the bulk flow to the channel walls while the outer layers generate eddies in close proximity to the membrane surface.

Although these modified spacers are able to markedly enhance the mass transfer, they inevitably increase the pressure drop through the membrane module, thereby resulting in higher energy consumption. Studies of spacer design [22] have rarely reported a higher mass-transfer coefficient while avoiding a significant increase in the pressure drop. Xie et al. [23] recently employed sinusoidal spacers in reverse osmosis (RO) processes, which were originally designed for heat exchangers [24]. It was expected that the sinusoidally shaped channels could reduce the hydrodynamic resistance owing to the smoother paths. However, a marked increase in the pressure drop was observed when the amplitude of the sinusoidal curve was increased and the wavelength was shortened to some critical values.

An interesting phenomenon in nature is that some organisms growing in flowing water usually develop flexible bodies that help them minimize hydrodynamic drag forces by deforming into a more streamlined shape. This is like a tree that bends itself in a strong wind. The underlying mechanisms of these phenomena that are related to the drag reduction through self-similar bending of a flexible body were experimentally and theoretically studied by Alben et al. [25] (a summary of their work is given by Steinberg [26]). Flexible structures usually undergo severe vibration (or flapping) due to the complex fluid-structure interactions as shown by several studies [27-30]. Taherzadeh et al. [31, 32] studied the behavior of the streamers in a biofilm and demonstrated that the oscillatory movement of the streamers is beneficial to the mass transfer in the biofilm. The aforementioned studies suggest that introducing some flexible structures into the

4

spacers in a membrane module might be a possible way to achieve a better balance between the mass-transfer enhancement and pressure loss.

The objective of the current work was to explore a conceptual design of spacers with hairy structures via a series of well-designed experiments. The vibrations of the fibers were observed using a high speed camera and mathematically analyzed over both time and frequency domains. Instead of aiming at completeness, the investigation was focused on the effects of fiber asymmetry and spacing. Prototypes with various fiber arrays were employed in a lab-scale forward osmosis (FO) process to evaluate the performance.

2. Experimental design and analysis

2.1 *System for observing the fiber vibrations and testing the filtration performance*

In order to observe the interactions between the fibers and flow, an acrylic filtration cell used for FO filtration was modified to accommodate a high speed camera. Fig. 1 shows a schematic of this dual function cell that can be used not only for the FO filtration but also for observing the vibrations of the hairy structures. Similar to that used in a previous study of the authors for non-invasive characterization via OCT [16], the central region of the top plate ($140\,\text{mm} \times 100\,\text{mm} \times 15\,\text{mm}$) of the filtration cell was replaced by a very thin glass window ($64\,\text{mm} \times 32\,\text{mm} \times 2\,\text{mm}$) as shown in Fig. 1 (a). Both the top and bottom plates had a fluid channel with the same size ($92\,\text{mm} \times 45\,\text{mm} \times 3.5\,\text{mm}$).

Fig. 1 (b) shows the framework that was designed for fixing the fibers in the fluid channel. This rectangular framework was composed of two lengthwise pieces with a width of $9.5\,\text{mm}$ and two transverse pieces with a width of $9\,\text{mm}$. The thickness of the

5

lengthwise pieces approximately matched the depth of the fluid channels ($3.5 \, \text{mm}$), whereas the transverse pieces had an indent of about $2.5 \, \text{mm}$ on the side facing the membrane so that the fluid could enter the channel with less resistance. Therefore, the effective cross-sectional area of the fluid channel was approximately $91 \times 10^{-6} \, \text{m}^2$ ($26 \, \text{mm} \times 3.5 \, \text{mm}$). The fibers were glued onto a disposable plastic strip ($91 \, \text{mm} \times 4 \, \text{mm} \times 0.5 \, \text{mm}$). This strip then was fixed into the framework by applying modeling clay to the indents so that the distance between the fibers and the membrane surface could be adjusted. In all the experiments the fibers were in close proximity to the membrane surface (varied from ~0.5 to 1.5 mm).

A high speed camera (Olympus, i-Speed LT) was employed to record the fiber vibrations and the combination of the dual function cell and the high speed camera is schematically shown in Fig. 2. A low temperature light source (Olympus, ILK-7A) was used to facilitate the video recording at a high frame rate. The top and bottom fluid channels were separated by an FO membrane (TFC-FO, water permeability ~2.6 LMH/bar, NaCl rejection ~94.8%, HTI, Albany, OR). Pure water was circulated through the top channel via a gear pump (Cole Parmer, 75211-35). The flow rate was fixed at approximately $3.2 \times 10^{-5} \, \text{m}^3/\text{s}$ (the Reynolds number based on the channel hydraulic diameter was 2415). For the vibration characterization no solution was pumped into the bottom channel. Instead, a glass plate with the same size as the channel was placed in the bottom channel such that the effective channel height for the hairy structures could be close to that used in a membrane module. In contrast, a salt solution (NaCl, $1 \, \text{mol/L}$) was circulated through the bottom channel as the draw solution during the FO filtration

6

experiments. The permeate flux was measured by weighing the tank containing the salt solution. Specially, the active layer of the FO membrane was exposed to the draw solution to reduce the effect of the internal concentration polarization (ICP) [33, 34]; the flow rate in each channel was set at the same level for all the filtration tests.

2.2 *Characterization of fiber vibrations*

One of the key steps to reveal the complex fluid-fiber interactions is to characterize the fiber vibrations under various conditions. The hairy structures are similar to a flexible cantilever beam whose free vibration consists of a series of modes associated with the corresponding natural frequencies. More complex vibration modes can occur when the beam is subject to dynamic external loads. In the current work the vibration characterization was implemented by analyzing the displacement of the fiber tip rather than the entire fiber.

The hairy structures were simulated using a segment of nylon thread with a nominal diameter D of $0.2\,\mathrm{mm}$. The elastic modulus E of this nylon thread, which was measured by an electromechanical system (MicroTester, Instron 5848), was approximately $0.09\,\mathrm{GPa}$, and its specific mass (mass per unit length) was approximately $3.5\times10^{-5}\,\mathrm{kg/m}$. Thread segments having a length $L\cong11\,\mathrm{mm}$ ($L/D\cong55$) were glued onto the strip to form a single fiber or a fiber array. The effects of the asymmetry were investigated by attaching an epoxy bead to the fiber tip. The diameter ratios of the bead to the fiber D_b/D were 3 and 7 for the small and large beads, respectively. The image samples (representative frames chosen from the video clips) of both the uniform (in the upper panels) and asymmetric fibers (in the lower panels) are shown in Fig. 3. Specially,

7

the semi-transparent fibers were marked at their tip and base with black color for digitally tracking the movement. The post-treatment of the images was implemented using MATLAB codes that were developed in-house.

The bending of the fibers was ignored in the analysis so that the displacement of the fiber tip could be characterized by a well-defined angular displacement. As shown in the left panels of Fig. 3, the fibers at rest are approximated by a dashed straight line segment with green color connecting the fiber tip and base. In all the experiments the initial position of the fibers was adjusted so that the axial direction of the fibers (i.e., the green dashed line) was approximately perpendicular to the direction of the bulk flow. At a certain instant, the fiber deviated from their initial position, and the instantaneous position is denoted by the dashed line segments with blue color in the middle panels of Fig. 3. The angle α between the green and blue line segments was defined as the absolute angular displacement.

The equilibrium position of the fiber during the vibration was different from its position at rest due to the effect of the flow. In this analysis this equilibrium position was approximately evaluated by averaging the absolute angular displacements over time (

$\bar{\alpha} = \sum_{i=1}^{n} \alpha_i \Big/ n$) and is denoted by the red line segments in the right panels of Fig. 3.

Therefore, the relative angular displacement θ was defined as the angle between the blue and red line segments. The major objective of the vibration characterization was to obtain the relative angular displacement as a function of time from the video clips. Each video clip recorded the fiber vibration for approximately $15\,\text{s}$ at a frame speed of $1000\,\text{fps}$. Moreover, one needs to note that the vibrations recorded by the high speed

8

camera are actually projections of the three-dimensional vibrations onto an optical plane that is perpendicular to the probe light. This limitation prevented analyzing possible vibration components in the direction parallel to the probe light. When the fiber is perpendicular to the bulk flow, the vibration analysis employed in the current work indicates the fiber fluctuations that are approximately aligned with the flow.

Three fiber configurations were employed in the current investigation. The basic configuration had a single fiber centered in the channel as shown in Fig. 4 (a). Two parallel fibers in a tandem arrangement constituted the second configuration as shown in Fig. 4 (b). The pitch ratio, which is the ratio between the fiber spacing and the fiber diameter L_s/D, was set at 4 for the short spacing cases and 10 for the long spacing cases. Fig. 4 (c) shows the fiber array for the third configuration. The basic pattern in this array involved four parallel fibers, which were separated into two tandem groups attached to the strips in an alternating pattern so that they partially nested into each other.

3. Experimental results and discussion

3.1 *Effects of fiber asymmetry and spacing on the vibrations*

Understanding the behavior of a single fiber in a fluid flow is of fundamental importance for designing the spacer with hairy structures. There could be many factors that have impact on the interactions between the fiber and fluid. As a starting point for this experimental investigation, the focus was on the effects of fiber asymmetry spacing. In this vibration characterization the tested fibers were positioned in the middle of the fluid channel with its axial direction perpendicular to the direction of the bulk flow. The movement of the fiber tip relative to its base was recorded by the high speed camera as

the crossflow rate was set at $3.2 \times 10^{-5}\ \mathrm{m^3/s}$. The duration of each observation was approximately $15\,\mathrm{s}$.

The asymmetry of a fiber was varied by attaching epoxy beads having different aspect ratios D_b/D 3 and 7 to the fiber tip and the characterization results were compared with those from the uniform fiber, i.e., the aspect ratio $D_b/D = 1$. The time series of the relative angular displacement are demonstrated in Fig. 5 for differently sized beads. It is evident that the asymmetric fibers gave rise to a vibration with markedly higher amplitudes than the uniform fiber. The variation in the vibration modes is directly associated with the change of the moment of inertia, which is caused by the bead in this case. Besides, the bead also increased the contact area between the fiber and the flow, thereby amplifying the intricate fiber-flow interactions. Nevertheless, the fiber with a larger bead ($D_b/D = 7$) is not notably superior to the one with a smaller bead ($D_b/D = 3$) as can be seen by comparing Fig. 5 (b) with Fig. 5 (c).

An important source of the vibration excitation in a fluid system is some flow instabilities associated with the structural motions [35], such as vortex shedding whose threshold is usually associated with the Reynolds number Re_D based on the diameter of the bluff body. It is generally accepted [36] that the critical value of Re_D is approximately 40, beyond which vortices begin to shed with a certain frequency. For the uniform fibers used in this study, the value of Re_D is approximately 78, which indicates that vortex shedding could be one of the mechanisms accounting for the fiber vibrations. The estimated value of the shedding frequency f_s is higher than $200\,\mathrm{Hz}$ in

terms of the correlation between the Strouhal number $St \equiv f_s D / u$ (u is the velocity of the free stream) and Re_D [37]. However, the spectral analysis shown in Fig. 6 (normalized energy spectral density (ESD) vs. frequency) does not indicate any component having frequencies in this region. Previous studies [38-42] revealed that vortices can also be formed at the free end and base region of the cantilevered structure. These end effects can significantly change the pattern of the vortices shed from the bulk body, thereby resulting in the so-called oblique shedding at a relatively low frequency. This is especially true when the cantilevered structure is flexible [28, 43, 44] and asymmetric (e.g., cylinders with end plates [45, 46]).

The hairy structures could be fiber arrays containing a number of fibers. It is expected that fiber combinations would have synergistic effects on the flow field. The basic unit in a fiber array consists of two fibers in a tandem arrangement as shown in Fig. 4 (b). The wake of the upstream fiber may have a significant influence on the vibrations of the downstream fiber, since the flow direction is normal to the axial direction of the fibers. In this study the investigation focused on the response of the downstream fiber while varying its position relative to the upstream fiber. The downstream fiber was positioned in the neighborhood of the upstream fiber for two different pitch ratios ($L_s / D = 4$ and 10). A single fiber can be viewed as the extreme case in which the distance between the upstream and downstream fibers is infinite. Therefore, the results for a single fiber are used as the baseline for comparison.

Two uniform fibers were employed in the tests and the vibration characterization was applied to the downstream fiber. The characterization results are plotted as the relative

11

angular displacement versus time in Fig. 7. These time series clearly indicate that the wake of the upstream fiber had a significant impact on the vibration behavior of the downstream fiber. In contrast to the result in Fig. 7 (a) for the single fiber, not only the vibration amplitudes of the downstream fiber but also the extent of the fluctuations was substantially increased when the spacing between the fibers was reduced from infinity to $L_s/D = 10$ as shown in Fig. 7 (b). However, a closer arrangement of $L_s/D = 4$ did not result in any discernible changes in the vibrations as indicated by Fig. 7 (c).

The vibrations of the downstream fiber were also analyzed based on the corresponding spectral decomposition, which is shown by plotting the normalized ESD versus frequency in Fig. 8. It shows that the bandwidth of the frequency is getting broader as the spacing is reduced. The vibration gains more high frequency components whereas the intensity of the low frequency components is decreased. In contrast to the spectrum for the long spacing case ($L_s/D = 10$), a strong peak at a frequency of $100\,\mathrm{Hz}$ is clearly observed in the spectrum for the short spacing case ($L_s/D = 4$). It is possible that this high frequency vibration was induced by some structure-related instability of the flow rather than the fluctuations in the free stream.

3.2 *Membrane performance tests with different fiber arrays*

The ultimate objective of using the hairy structures is to enhance membrane flux by increasing the mass-transfer coefficient in the vicinity of the membrane surface. One of the advantages of using hairy spacers is that the fibers can be placed at a position extremely close to the membrane surface as can be seen in this work (less than $1\,\mathrm{mm}$ for a uniform fiber). It was expected that the concentration boundary layer could be directly

disturbed by the vibration of the fibers. In order to verify the effect of the fiber vibration on the mass transfer, fiber arrays composed of more fibers were fabricated and used in the FO tests.

Intuitively, flexible fibers are superior to rigid fibers that cannot be excited by the flow. It is nevertheless worthwhile to examine the difference resulting from the vibration of flexible structures. Following this idea, rigid fibers were approximated by stretching the segments of nylon thread across the width of the channel as taut as possible. The pitch ratio was set at 10 so as to form approximately 40 stretched strings. After being used to test the performance during FO, these strings were cut at one end to form the fiber pattern as shown in Fig. 4 (c). This fiber array served as a prototype of the spacer with hairy structures in the FO tests. Epoxy beads ($D_b/D = 3$) then were attached onto the fiber tips, and the FO test was repeated with this spacer prototype having asymmetric fibers. Each of these spacer prototypes was duplicated for conducting repeat tests so that the evaluation of the filtration performance could be done in a statistical fashion.

The permeate flux for the FO was measured for each spacer prototype and the results are compared in Fig. 9. These results were normalized in relation to the case with the taut strings. It shows that the permeate flux was marginally increased when the stretched strings were turned into free fibers. However, the confidence interval for the case with the uniform fibers overlaps that of the case with the taut strings. In spite of the measurement uncertainties, it indicates that the change resulting from the vibration of the uniform fibers is not stable or strong enough to confirm any advantage of using the hairy structures. When the asymmetry of the fibers was increased by attaching the beads, the

13

filtration flux was significantly increased in comparison to the cases with the taut strings and uniform fibers.

In order to better understand the mechanisms underlying the variation in the filtration flux, the vibration characterization was applied to a fiber approximately centered in the array. The vibrations of the uniform and asymmetric fibers are plotted as a time series in Fig. 10 and the corresponding spectral decomposition in Fig. 11. In comparison with the case of two uniform fibers, the time history of the uniform fiber in the array exhibits vibrations with relatively small amplitudes as shown in Fig. 10 (a), and some high intensity components are found within the low frequency regime in Fig. 11 (a). The most significant changes are observed for the array with the asymmetric fibers. As clearly shown in Fig. 10 (b), large amplitude fluctuations are frequently found in the time series. These impulse-like signals result in more high intensity components at very high frequencies (even higher than $100\,\mathrm{Hz}$) according to the spectral decomposition in Fig. 11 (b). It is reasonable to infer that these random vibrations could promote the turbulence in the region very close to the membrane surface, where the salt concentration was increased owing to the back diffusion of salt from the draw solution and thereby reduced the driving force (i.e., the osmotic pressure difference). The increase in turbulence within the concentration boundary layer would improve the mass transfer near the membrane surface, i.e., a higher mass-transfer coefficient, thereby mitigating the external concentration polarization on the feed solution side. Note that the efficiency of FO processes is mainly limited by the internal concentration polarization, which may not be significantly affected by the disturbances outside the membrane structure. Therefore, it is expected that more significant improvement would be achievable when applying the

hairy structures to an RO process, whose efficiency is dominated by the external concentration polarization.

4. Implications and perspectives

Novel hairy spacers were developed for the first time. Unlike conventional spacers that are rigid in shape and remain static under crossflow conditions (i.e., passive turbulence promoters), flexible fibers can be used to form hair-like structures as shown by this work. The fiber vibrations induced by the crossflow conditions can effectively promote mass transfer in membrane flow channels. In this regard, the current study opens a new paradigm for "activated" spacer design.

The spacer prototypes used in this conceptual design were in a form having minimal effects of the framework for fixing the fibers. For more realistic designs the framework can be a spacer with conventional or novel structures. Well-designed combinations of the framework and fibers may further enhance the membrane performance in a synergistic way. Such designs will involve more intricate considerations, such as the geometry, material, and orientation of the fibers, the structure of the framework, and others. Spacer asymmetry was achieved in this study by attaching a small bead to the end of the fiber. For practical applications, more nonlinear structures (e.g., curved fibers, fibers with the free end enlarged, and fibers with flakes attached to it) could be employed to achieve similar or better performance. The advancement of three-dimensional printing techniques will enable such structures to be fabricated at moderate cost.

Hairy structures may also be able to mitigate membrane fouling since the fluid instabilities caused by fiber vibrations should prevent or reduce the deposition of the

15

fouling particles on the membrane surface. Although the pressure loss was not examined in this study due to limitations of the lab-scale filtration module, it is likely that less pressure drop would be caused by the flexible fibers in comparison to the thicker fixed filaments in conventional spacers. This is to be examined in further work.

5. Summary and conclusions

A conceptual design of spacers with hairy structures was presented in this paper. The vibration behavior of the flexible fibers was investigated using a custom-designed experiment platform combining a high speed camera and an FO membrane system. The characterization results were interpreted by both time-series and spectral analyses. The following conclusions can be drawn from the experimental results:

(i) The intensity of the vibrations can be improved by increasing the asymmetry of the fiber, though the improvement is limited in some regimes;

(ii) The vibration of a fiber can be significantly affected by the neighboring fibers; the coupling effects can be well-controlled by varying the spacing;

(iii) The fiber arrays can effectively disturb the concentration field near the membrane surface; the mass-transfer rate can be substantially enhanced when severe fiber vibrations are excited.

In addition, the underlying mechanisms accounting for the complex fiber-flow interactions were analyzed on the basis of the vibration characterization. The characterization results indicate that vortex shedding could be mainly responsible for the dynamic behavior of the fibers. More detailed and rigorous investigation is required to further develop the spacers with hairy structures.

16

Acknowledgments

References

[1] C.P. Koutsou, S.G. Yiantsios, A.J. Karabelas, Numerical simulation of the flow in a plane-channel containing a periodic array of cylindrical turbulence promoters, J. Membr. Sci., 231 (2004) 81-90.

[2] J. Schwinge, P.R. Neal, D.E. Wiley, D.F. Fletcher, A.G. Fane, Spiral wound modules and spacers: Review and analysis, J. Membr. Sci., 242 (2004) 129-153.

[3] A.R. Dacosta, A.G. Fane, D.E. Wiley, Spacer characterization and pressure drop modelling in spacer-filled channels for ultrafiltration, J. Membr. Sci., 87 (1994) 79-98.

[4] G. Schock, A. Miquel, Mass-transfer and pressure loss in spiral wound modules, Desalination, 64 (1987) 339-352.

[5] C.C. Zimmerer, V. Kottke, Effects of spacer geometry on pressure drop, mass transfer, mixing behavior, and residence time distribution, Desalination, 104 (1996) 129-134.

[6] Z. Cao, D.E. Wiley, A.G. Fane, CFD simulations of net-type turbulence promoters in a narrow channel, J. Membr. Sci., 185 (2001) 157-176.

[7] S.K. Karode, A. Kumar, Flow visualization through spacer filled channels by computational fluid dynamics I. Pressure drop and shear rate calculations for flat sheet geometry, J. Membr. Sci., 193 (2001) 69-84.

[8] J. Schwinge, D.E. Wiley, D.F. Fletcher, Simulation of the flow around spacer filaments between narrow channel walls. 1. Hydrodynamics, Ind. Eng. Chem. Res., 41 (2002) 2977-2987.

[9] J. Schwinge, D.E. Wiley, D.F. Fletcher, Simulation of the flow around spacer filaments between channel walls. 2. Mass-transfer enhancement, Ind. Eng. Chem. Res., 41 (2002) 4879-4888.

[10] L.F. Song, S.W. Ma, Numerical studies of the impact of spacer geometry on concentration polarization in spiral wound membrane modules, Ind. Eng. Chem. Res., 44 (2005) 7638-7645.

[11] A. Subramani, S. Kim, E.M.V. Hoek, Pressure, flow, and concentration profiles in open and spacer-filled membrane channels, J. Membr. Sci., 277 (2006) 7-17.

[12] S. Wardeh, H.P. Morvan, CFD simulations of flow and concentration polarization in spacer-filled channels for application to water desalination, Chem. Eng. Res. Des., 86 (2008) 1107-1116.

[13] Y.L. Li, K.L. Tung, Y.S. Chen, K.J. Hwang, CFD analysis of the initial stages of particle deposition in spiral-wound membrane modules, Desalination, 287 (2012) 200-208.

[14] M. Amokrane, D. Sadaoui, C.P. Koutsou, A.J. Karabelas, M. Dudeck, A study of flow field and concentration polarization evolution in membrane channels with two-dimensional spacers during water desalination, J. Membr. Sci., 477 (2015) 139-150.

[15] P. Willems, N.G. Deen, A.J.B. Kemperman, R.G.H. Lammertink, M. Wessling, M.V. Annaland, J.A.M. Kuipers, W.G.J. van der Meer, Use of Particle Imaging Velocimetry to measure liquid velocity profiles in liquid and liquid/gas flows through spacer filled channels, J. Membr. Sci., 362 (2010) 143-153.

[16] Y. Gao, S. Haavisto, C.Y. Tang, J. Salmela, W. Li, Characterization of fluid dynamics in spacer-filled channels for membrane filtration using Doppler optical coherence tomography, J. Membr. Sci., 448 (2013) 198-208.

[17] A. Dewan, P. Mahanta, K.S. Raju, P.S. Kumar, Review of passive heat transfer augmentation techniques, Proc. Inst. Mech. Eng. Part A-J. Power Energy, 218 (2004) 509-527.

[18] S. Eiamsa-Ard, P. Promvonge, Enhancement of heat transfer in a tube with regularly-spaced helical tape swirl generators, Sol. Energy, 78 (2005) 483-494.

[19] J. Schwinge, D.E. Wiley, A.G. Fane, Novel spacer design improves observed flux, J. Membr. Sci., 229 (2004) 53-61.

[20] J. Balster, I. Punt, D.F. Stamatialis, A. Wessling, Multi-layer spacer geometries with improved mass transport, J. Membr. Sci., 282 (2006) 351-361.

[21] F. Li, W. Meindersma, A.B. de Haan, T. Reith, Novel spacers for mass transfer enhancement in membrane separations, J. Membr. Sci., 253 (2005) 1-12.

[22] G.A. Fimbres-Weihs, D.E. Wiley, Review of 3D CFD modeling of flow and mass transfer in narrow spacer-filled channels in membrane modules, Chem. Eng. Process., 49 (2010) 759-781.

[23] P. Xie, L.C. Murdoch, D.A. Ladner, Hydrodynamics of sinusoidal spacers for improved reverse osmosis performance, J. Membr. Sci., 453 (2014) 92-99.

[24] H.M. Metwally, R.M. Manglik, Enhanced heat transfer due to curvature-induced lateral vortices in laminar flows in sinusoidal corrugated-plate channels, Int. J. Heat Mass Transf., 47 (2004) 2283-2292.

[25] S. Alben, M. Shelley, J. Zhang, Drag reduction through self-similar bending of a flexible body, Nature, 420 (2002) 479-481.

[26] V. Steinberg, Hydrodynamics - Bend and survive, Nature, 420 (2002) 473-473.

[27] M.J. Shelley, J. Zhang, Flapping and Bending Bodies Interacting with Fluid Flows, in: S.H. Davis, P. Moin (Eds.) Annual Review of Fluid Mechanics, Vol 43, 2011, pp. 449-465.

[28] L.D. Zhu, Viscous flow past a flexible fibre tethered at its centre point: vortex shedding, J. Fluid Mech., 587 (2007) 217-234.

[29] L.D. Zhu, Interaction of two tandem deformable bodies in a viscous incompressible flow, J. Fluid Mech., 635 (2009) 455-475.

[30] L.D. Zhu, C.S. Peskin, Drag of a flexible fiber in a 2D moving viscous fluid, Computers & Fluids, 36 (2007) 398-406.

[31] D. Taherzadeh, C. Picioreanu, H. Horn, Mass Transfer Enhancement in Moving Biofilm Structures, Biophys. J., 102 (2012) 1483-1492.

[32] D. Taherzadeh, C. Picioreanu, U. Kuttler, A. Simone, W.A. Wall, H. Horn, Computational Study of the Drag and Oscillatory Movement of Biofilm Streamers in Fast Flows, Biotechnol. Bioeng., 105 (2010) 600-610.

[33] W. Li, Y. Gao, C.Y. Tang, Network modeling for studying the effect of support structure on internal concentration polarization during forward osmosis: Model development and theoretical analysis with FEM, J. Membr. Sci., 379 (2011) 307-321.

[34] C.Y.Y. Tang, Q.H. She, W.C.L. Lay, R. Wang, A.G. Fane, Coupled effects of internal concentration polarization and fouling on flux behavior of forward osmosis membranes during humic acid filtration, J. Membr. Sci., 354 (2010) 123-133.

[35] E.R. Naudascher, D., Flow-Induced Vibrations: An Engineering Guide, Dover Publications, Mineola, NY, 2005.

[36] R.D. Blevins, Flow-Induced Vibration, 1st ed., Van Nostrand Reinhold company, New York, NY, USA, 1977.

[37] U. Fey, M. Konig, H. Eckelmann, A new Strouhal-Reynolds-number relationship for the circular cylinder in the range 47 < Re < 2x10(5), Physics of Fluids, 10 (1998) 1547-1549.

[38] S. Behara, S. Mittal, Flow past a circular cylinder at low Reynolds number: Oblique vortex shedding, Physics of Fluids, 22 (2010).

[39] C.H.K. Williamson, Three-dimensional vortex dynamics in bluff body wakes, Experimental Thermal and Fluid Science, 12 (1996) 150-168.

[40] C.H.K. Williamson, Vortex dynamics in the cylinder wake, Annu. Rev. Fluid Mech., 28 (1996) 477-539.

[41] A.L.C. Fujarra, C.P. Pesce, F. Flemming, C.H.K. Williamson, Vortex-induced vibration of a flexible cantelever, J. Fluids Struct., 15 (2001) 651-658.

[42] C.T. Yamamoto, J.R. Meneghini, F. Saltara, R.A. Fregonesi, J.A. Ferrari Jr, Numerical simulations of vortex-induced vibration on flexible cylinders, J. Fluids Struct., 19 (2004) 467-489.

[43] J.K. Shang, A.J. Smits, H.A. Stone, The appearance of P plus S modes in the wake of a freely vibrating, highly flexible cylinder, J. Fluids Struct., 43 (2013) 481-486.

[44] J. Revstedt, Interaction between an incompressible flow and elastic cantilevers of circular cross-section, Int. J. Heat Fluid Flow, 43 (2013) 244-250.

[45] D. Gerich, H. Eckelmann, Influence of end plates and free ends on the shedding frequency of circular-cylinders, J. Fluid Mech., 122 (1982) 109-121.

[46] S. Szepessy, P.W. Bearman, Aspect ratio and end plate effects on vortex shedding from a circular-cylinder, J. Fluid Mech., 234 (1992) 191-217.

Figure Legends

Figure 1 Schematic of the dual function cell for the vibration characterization and FO filtration: (a) the structure of the top plate (with the observation window) and the bottom plate; (b) the framework for fixing the fibers. Both plates have a fluid channel with the same geometry.

Figure 2 Schematic of the experiment system for the vibration characterization. The fiber vibrations were observed using the high speed camera. During the vibration characterization, pure water was circulated through the top channel filled with the framework carrying the fibers whereas the bottom channel was filled with a glass plate. During the FO filtration evaluation, both the channels were filled with the same spacer

prototypes, and the feed and draw solutions were circulated through the respective channels in opposite directions.

Figure 3 Typical fiber images from the high speed camera showing the definitions of the quantities used in the vibration characterization. The upper panels are for the uniform fiber while the lower panels show the asymmetric fiber formed by attaching an epoxy bead onto the fiber tip. The tip and base of the fibers are marked by black color for tracking the movement in the post-treatment. The green dashed line segments indicate the position for the fiber at rest; the blue dashed line segments denote the fiber position at any instant during the vibration; the red dashed line segments indicate the equilibrium position that was calculated by averaging the instantaneous positions over time. The absolute angular displacement was defined as the angle α between the blue and green dashed line segments while the relative angular displacement was the angle θ between the blue and red dashed line segments.

Figure 4 Schematic of the fiber configurations: (a) a single fiber centered in the channel; (b) two fibers in tandem arrangement; (c) fiber array with fiber bundles (containing two fibers) alternately attached to the opposite borders of the channel. The direction of the bulk flow was normal to the axial direction of the fibers.

Figure 5 Characteristic time series of the vibrations of a single fiber while varying the fiber asymmetry. The asymmetric fibers were formed by attaching an epoxy bead onto the fiber tip, and the asymmetry is characterized by the diameter ratio of the bead to the fiber D_b/D. The vibrations are described by the time history of the relative angular displacement, which is the deviation of the instantaneous angle from the equilibrium position.

Figure 6 Spectral decompositions of the vibrations of a single fiber while varying the fiber asymmetry. The asymmetric fibers were formed by attaching an epoxy bead onto the fiber tip, and the asymmetry is characterized by the diameter ratio of the bead to the fiber D_b/D. The energy spectral density was normalized and plotted by using a drop line at each frequency.

Figure 7 Characteristic time series of the vibrations of a fiber downstream of another fiber while varying the pitch ratio L_s/D. Both the fibers were uniform, and the flow rate was $3.2 \times 10^{-5} \text{ m}^3/\text{s}$. The vibrations are described by the time history of the relative angular displacement, which is the deviation of the instantaneous angle from the equilibrium position.

Figure 8 Spectral decompositions of the vibrations of a fiber downstream of another fiber while varying the pitch ratio L_s/D. Both the fibers were uniform and the flow rate was $3.2 \times 10^{-5} \text{ m}^3/\text{s}$. The energy spectral density was normalized and plotted by using a drop line at each frequency.

Figure 9 Comparison of the permeate fluxes of the FO filtration with various spacer prototypes. The spacer prototypes contained about 40 fibers (including taut strings, uniform fibers and asymmetric fibers with $D_b/D = 3$) fixed onto the framework in terms of the pattern in Fig. 4 (c). During the tests, both the top and bottom channels were filled with the same spacer prototypes. The flow rate was $3.2 \times 10^{-5} \text{ m}^3/\text{s}$ in each channel. The experimental results were normalized by the mean of the filtration flux from the case with the taut strings in the channel.

Figure 10 Characteristic time series of the vibrations of the central fiber in the arrays with uniform fibers and asymmetric fibers ($D_b/D = 3$). The fiber arrays contained about 40 fibers fixed onto the framework in terms of the pattern in Fig. 4 (c). The flow rate was $3.2 \times 10^{-5} \text{ m}^3/\text{s}$. The vibrations are described by the time history of the relative angular displacement, which is the deviation of the instantaneous angle from the equilibrium position.

Figure 11 Spectral decompositions of the vibrations of the central fiber in the arrays with uniform fibers and asymmetric fibers ($D_b/D = 3$). The fiber arrays contained about 40 fibers fixed onto the framework in terms of the pattern in Fig. 4 (c). The flow rate was $3.2 \times 10^{-5} \text{ m}^3/\text{s}$. The energy spectral density was normalized and plotted by using a drop line at each frequency.

21

Research Highlights

- Novel spacers with hairy structures were explored for enhancing the performance of membrane processes.
- Experimental study was carried out using the prototypes to verify and optimize the dynamic responses of the hairy structures to the flow.
- Performance tests using the prototypes in an FO process imply that this novel spacer design could significantly improve the efficiency of membrane processes.
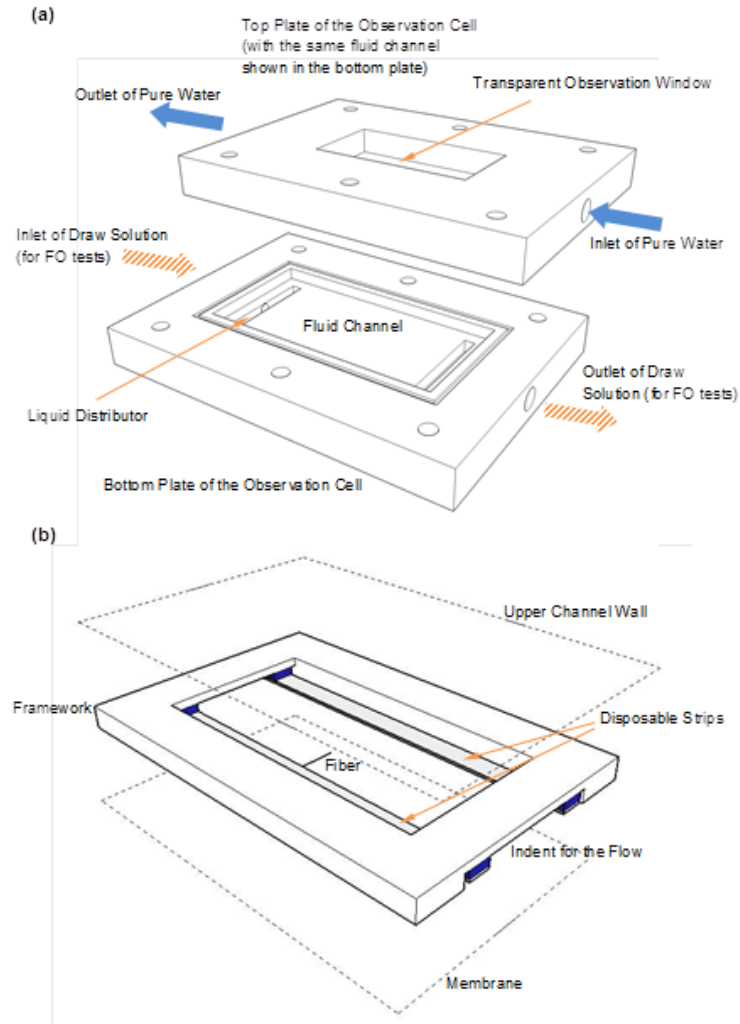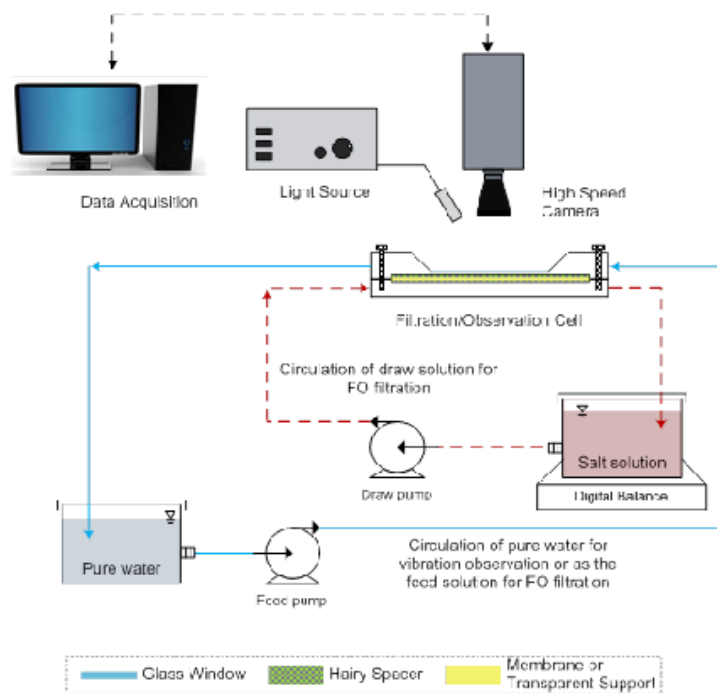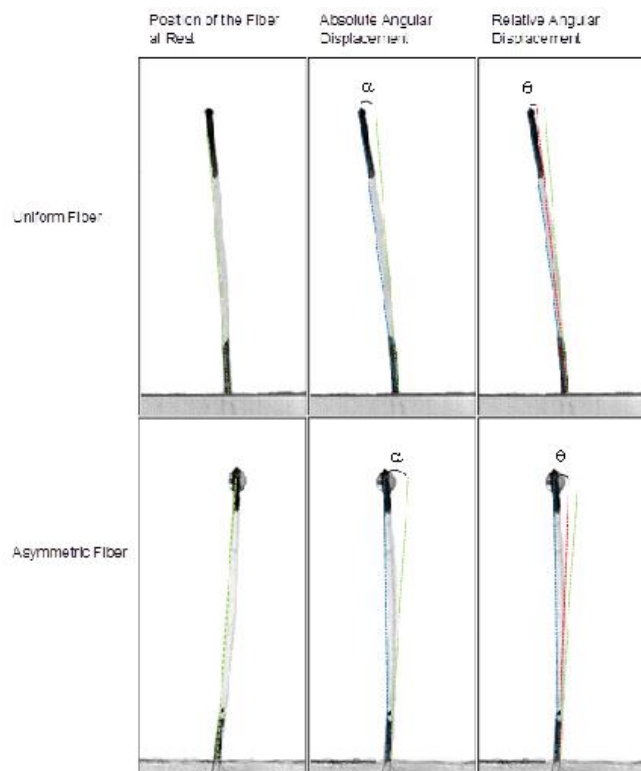
(a)

Top Plate of the Observation Cell
(with the same fluid channel
shown in the bottom plate)

Transparent Observation Window

Outlet of Pure Water

Inlet of Draw Solution
(for FO tests)

Inlet of Pure Water

Fluid Channel

Outlet of Draw
Solution (for FO tests)

Liquid Distributor

Bottom Plate of the Observation Cell

(b)

Upper Channel Wall

Framework

Disposable Strips

Fiber

Indent for the Flow

Membrane

fig 1

fig 2

fig 3

Single Fiber

(a)

Bulk Flow

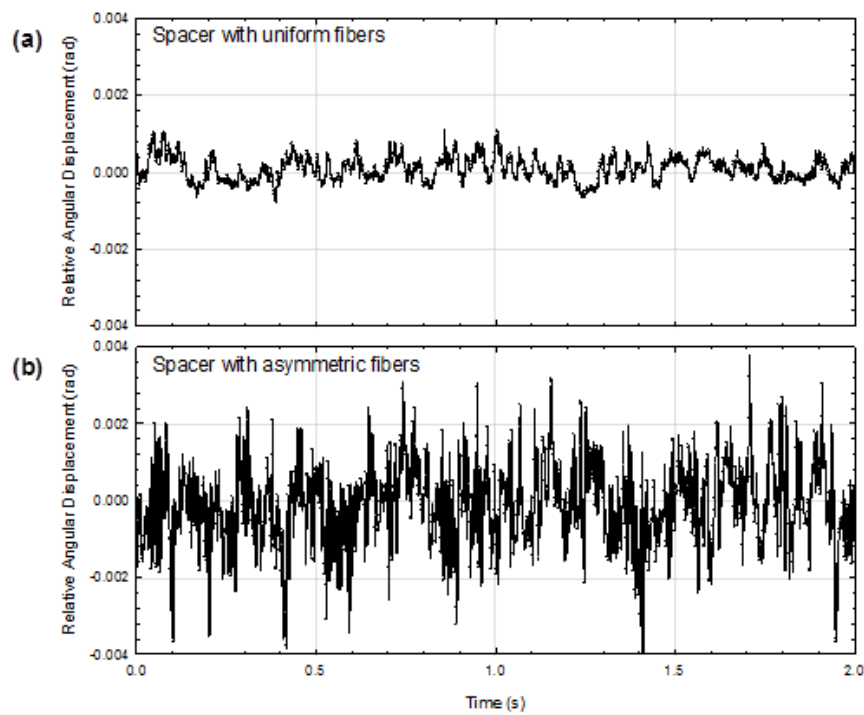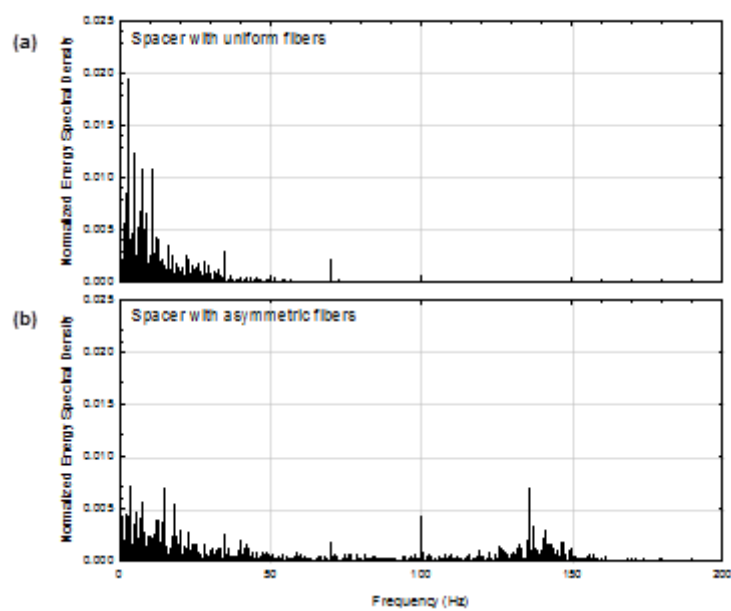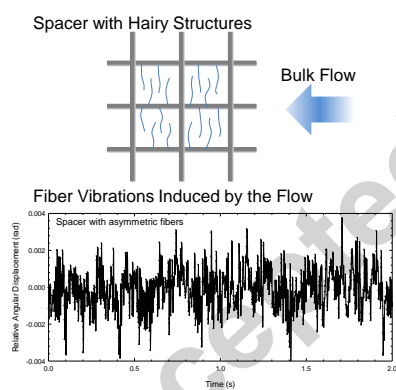Two Fibers in Tandem Arrangement

(b)

Fiber Array

(c)

fig 4

fig 5

fig 6

fig 7

fig 8

fig 9

fig 10

fig 11

graphical abstract